

Article

The Modification of Pt/Graphene Composites with Oxophilic Metal Bi (Bi_2O_3) and Its Dual-Functional Electro-Photo Catalytic Performance

Yingli Wu ^{1,†}, Xiuyun Duan ^{1,†}, Zhongshui Li ^{1,2}, Shuhong Xu ¹, Yixin Xie ¹, Yufei Lai ¹ and Shen Lin ^{1,2,*}

¹ College of Chemistry & Materials Science, Fujian Normal University, Fuzhou 350007, China; annayl@163.com (Y.W.); siuwuen@163.com (X.D.); zslifjnu.edu.cn (Z.L.); xushuhongxu@gmail.com (S.X.); xieyixinxieyixin@163.com (Y.X.); fjscLYF@163.com (Y.L.)

² Fujian Provincial Key Laboratory of Advanced Materials Oriented Chemical Engineering, Fuzhou 350007, China

* Correspondence: shenlin@fjnu.edu.cn; Tel.: +86-591-2286-7399

† These authors contributed equally to this work.

Received: 16 August 2018; Accepted: 28 September 2018; Published: 17 October 2018



Abstract: The Pt-Bi (Bi_2O_3)/GNs (PVP) composite was synthesized using aqueous solution synthesis and characterized by transmission electron microscopy (TEM), X-ray diffraction (XRD), X-ray photoelectron spectroscopy (XPS), inductively coupled plasma-atomic emission spectroscopy (ICP-AES) and Raman spectroscopy. It was found that the water-soluble polyvinyl pyrrolidone (PVP) helped to tune the particles' morphology, resulting in a uniform distribution of Pt-Bi nanoclusters on the surface of graphene. Cyclic voltammetry, chronoamperometry and linear scanning voltammetry (LSV) were used to study the electrocatalytic properties towards a methanol oxidation reaction (MOR) and an oxygen reduction reaction (ORR). The results show that Pt-Bi (Bi_2O_3)/GNs (PVP) exhibits superior bifunctional electrocatalytic properties for both MOR and ORR, mainly due to the introduction of oxophilic Bi species and the better dispersion of the Pt-Bi nanoclusters. In particular, the electro-photo catalysis for both MOR and ORR occurred under simulated sunlight irradiation due to the existence of photo-responsive Bi species, which is helpful for converting solar energy into electric energy during a traditional electrocatalytic process.

Keywords: Pt-Bi bimetal; electro-photo catalysis; methanol oxidation; oxygen reduction; alkaline medium

1. Introduction

Fuel cells have a wide range of applications in our daily life because they can transform the chemical energy of fuel into electricity through electrochemical reactions directly. Platinum (Pt) is employed as the most effective major catalysts due to its distinct chemical and electronic properties up to present [1–3]. Nevertheless, it is still a long way to realize the wide application of Pt catalysts due to its high cost, rare source, and sluggish kinetics [4]. Therefore, it is necessary to find more cost-effective and efficient alternatives.

Many efforts have recently been focused on Pt-based bimetallic catalysts because they can improve their electrocatalytic activity via a bifunctional mechanism or an electronic effect [5] and effectively reduce the usage of noble platinum. For example, PtRu [6], PtPd [7], and PtAu [8] have their own high activity in catalyzing methanol electro-oxidation. However, the introduction of Ru, Pd, or Au can not strongly overcome the fatal disadvantage of a Pt-based catalysts' high price. To this day, it has been reported that some cheap metals applied to a Pt-based catalyst can reduce the costs and increase the

activity [9], such as Pt-Cu [10], Pt-Co [11], Pt-Fe [12], Pt-Ni [13,14], and Pt-Bi [15]. Ding [16] reported a core-shell Ni@Pt catalyst and found that the unique structure and the electronic effects of the various metals were responsible for its high electrocatalytic performances. Peng [17] presented a one-pot hydrothermal synthesis of a Pt-Cu catalyst, which exhibited an enhanced catalytic performance due to the appropriately modified electron structure of Pt by alloying with Cu. Kannan [18] prepared a FePt/RGO bifunctional catalyst towards ORR and MOR and the oxophilic Fe played an important role in its bifunctional catalytic performances. Qin [19] synthesized a Pt-Co nano-crystal catalyst, which presented enhanced catalytic properties for the formic acid oxidation reaction (FOR) and ORR. It can be inferred that the electronic effects between Pt and the second metal are one of the main driving forces for their enhanced performances. The tolerance to CO poisoning of the Pt-based catalysts can be improved by increasing the oxide species among Pt-M bimetal's surface due to the oxophilic properties of the second cheap metal [20], which may be the other force for improving the performance.

Considering the favorable properties of the non-noble Bi in inhibiting CO poison effects [21] and the efficient photo-responsive properties of Bi oxide [22], Pt-Bi bimetal is expected to exhibit synergistic effects of photo- and electro-catalysis under light irradiation, which is similar to a Pt-semiconductor metal oxide such as TiO₂ [22], SnO₂ [23], or ZnO [24]. However, bismuth is easily lost during electrocatalysis and their morphologies are difficult to control due to the oxophilic property of the Bi species. Therefore, an appropriate support material, such as graphene nanosheets (GNs) and an effective morphology controlling agent, such as a water-soluble polymer are indispensable. We have previously reported an etched Pt-Bi (Bi₂O₃)/GNs (Etching) catalyst, which exhibited superior electrocatalysis than the commercial catalysts for catalyzing methanol oxidation [25]. However, the etching process removed most of the Bi species, which made Pt-Bi (Bi₂O₃)/GNs (Etching) lose the capacity of electro-photo synergistic catalysis under irradiation. So how to take advantage of the photo-responsive properties of Bi oxide in electrocatalysis is of significance and is interesting work.

In this work, a Pt-Bi (Bi₂O₃)/GNs (PVP) composite was synthesized using a facile wet chemical procedure, in which graphene nanosheets were used to support the Pt-Bi bimetal and their morphologies were controlled using an aqueous soluble polyvinyl pyrrolidone (PVP). As a result, Pt-Bi nanoparticles were uniformly distributed on the surface of the GNs and Pt-Bi (Bi₂O₃)/GNs (PVP) exhibited superior electrocatalytic properties towards the methanol oxidation reaction (MOR) and the oxygen reduction reaction (ORR). In particular, the Pt-Bi (Bi₂O₃)/GNs (PVP) composite had an electro-photo synergistic catalytic effect on catalyzing the MOR and the ORR under simulated sunlight irradiation due to the existence of the photosensitive species (Bi₂O₃), which harvests the simulator sunlight to assist electrocatalysts to convert chemical energy into electric energy.

2. Results and Discussion

2.1. Characterization

Figure 1A shows the X-ray diffraction (XRD) patterns of Pt-Bi (Bi₂O₃)/GNs (PVP) (curve a), Pt/GNs (PVP) (curve b) and Pt-Bi (Bi₂O₃)/GNs (curve c). The characteristic diffraction peaks located at 39.7°, 46.5°, 67.5° and 81.4° originated from (111), (200), (220) and (311) crystal planes of face-centered cubic (fcc) Pt [26]. The additional diffraction peak at 2θ of about 28.4° corresponds to the (121) plane of Bi₂O₃ [27] (curve a, c), indicating that the bismuth species in the composite mainly exists in the form of Bi₂O₃. Furthermore, the peak at 24.0° in curve b was assigned to the (002) crystal plane of carbon in graphene [28].

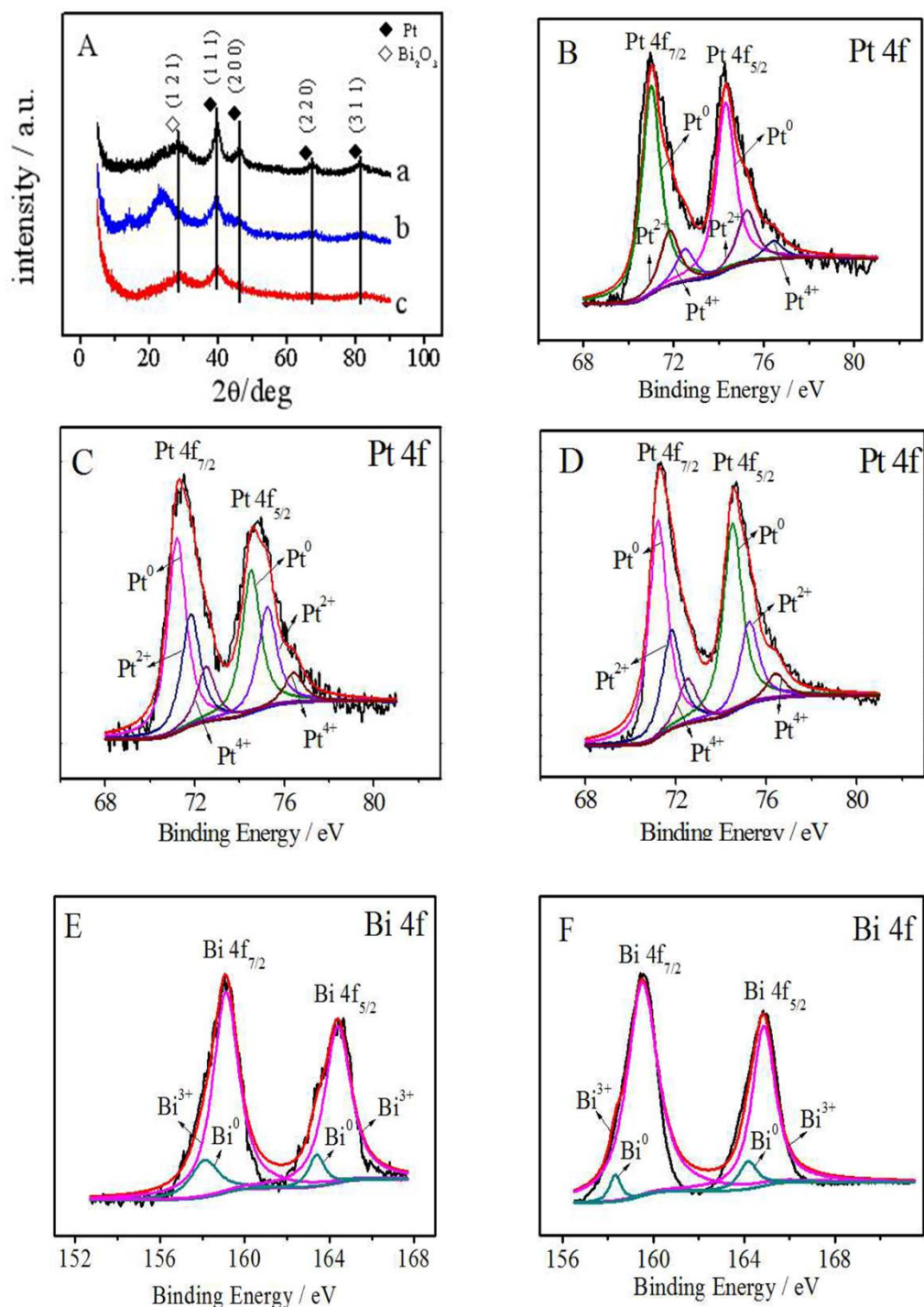


Figure 1. (A) X-ray diffraction (XRD) patterns: Pt-Bi (Bi_2O_3)/GNs (PVP) (a), Pt/GNs (PVP) (b), and Pt-Bi (Bi_2O_3)/GNs (c); (B) Pt 4f X-ray photoelectron spectroscopy (XPS) for Pt-Bi (Bi_2O_3)/GNs (PVP); (C) Pt 4f XPS for Pt/GNs (PVP); (D) Pt 4f XPS for Pt-Bi (Bi_2O_3)/GNs; (E) Bi 4f XPS for Pt-Bi (Bi_2O_3)/GNs (PVP); (F) Bi 4f XPS for Pt-Bi (Bi_2O_3)/GNs.

The composite was further characterized by XPS. As can be seen from Figure 1B–D, the Pt 4f signal was fitted using a non-linear least-square regression method and Shirley-type background corrections and Gaussian–Lorentzian peak shapes were used. It seems that the Pt species existed in various states because the Pt 4f signal was composed of three pairs of doublets. The most intense doublet (71.40 eV and 74.52 eV) was ascribed to metallic Pt (0) [29,30]. The doublet (71.83 eV and 75.24 eV) can be attributed to the Pt (II) chemical state (PtO or Pt(OH)₂) [30,31]. The weak doublet

(72.51 eV and 76.42 eV) can be assigned to the Pt (IV) chemical state (PtO_2) [30]. It was evident that the predominant species of Pt in the Pt-based catalysts above was metallic Pt. The fitted Bi 4f spectra of Pt-Bi (Bi_2O_3)/GNs (PVP) and Pt-Bi (Bi_2O_3)/GNs are shown in Figure 1E,F. The Bi 4f binding energies assigned to Bi (0) and Bi (III) were observed both in Pt-Bi (Bi_2O_3)/GNs (PVP) and Pt-Bi (Bi_2O_3)/GNs. After curve fitting, the peaks at 159.5 and 164.9 eV belong to the Bi (III) species (Bi_2O_3) and the peaks at 158.3 and 163.7 eV were due to the Bi (0) species [20,32]. It can be found from the peak intensity and the peak area that bismuth mainly existed in the form of Bi_2O_3 , which may be because Bi (0) is easily oxidized during the synthetic process due to its oxophilic property [33,34].

The morphologies of Pt-Bi (Bi_2O_3)/GNs (PVP), Pt/GNs (PVP), and Pt-Bi (Bi_2O_3)/GNs were analyzed by TEM. As shown in Figure 2A,B, Pt-Bi nanoclusters in Pt-Bi (Bi_2O_3)/GNs (PVP) were uniformly distributed on the surface of graphene and no obvious aggregation was observed between the clusters. However, the Pt-Bi particles in Pt-Bi (Bi_2O_3)/GNs were unevenly distributed on the graphene layer (Figure 2G) and some particles aggregated into irregular clusters (Figure 2H). In contrast, it can be concluded that PVP played a role in tuning the morphology of the particles supported on graphene, which is also verified by Figure 2D,E. As shown in Figure 3D,E, the Pt particles in Pt/GNs (PVP) exhibited a uniform distribution on the surface of the graphene due to the introduction of PVP.

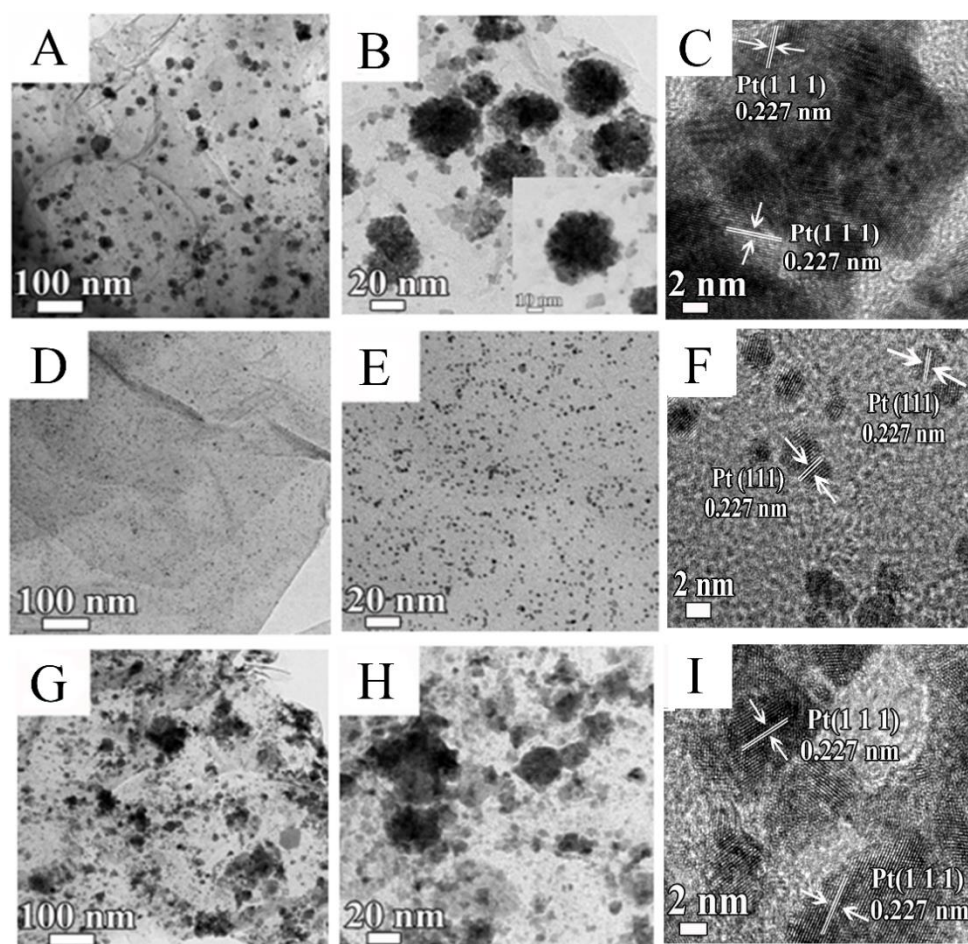


Figure 2. Transmission electron microscopy (TEM) images: Pt-Bi (Bi_2O_3)/GNs (PVP) (A,B), Pt/GNs (PVP) (D,E) and Pt-Bi (Bi_2O_3)/GNs (G,H); The inset in panel B is magnified TEM images of Pt-Bi (Bi_2O_3)/GNs (PVP); High-resolution transmission electron microscopy (HRTEM) images: Pt-Bi(Bi_2O_3)/GNs (PVP) (C), Pt/GNs (PVP) (F) and Pt-Bi (Bi_2O_3)/GNs (I).

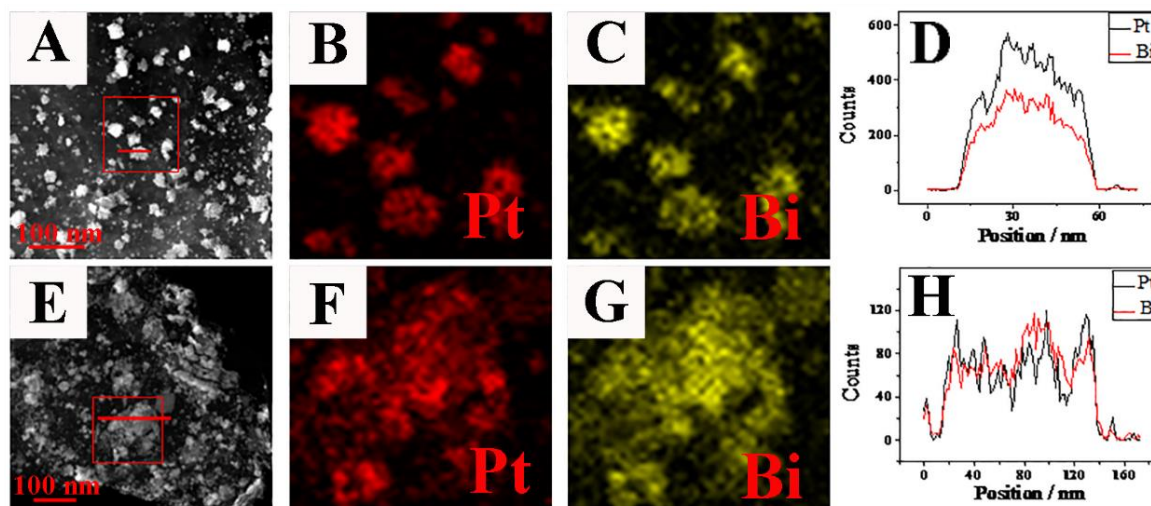


Figure 3. The high-angle annular dark-field scanning transmission electron microscopy (HAADF-STEM) images: Pt-Bi (Bi_2O_3)/GNs (PVP) (A), Pt-Bi (Bi_2O_3)/GNs (E); Elemental mapping images: Pt (B) and Bi (C) for Pt-Bi (Bi_2O_3)/GNs (PVP), Pt (F) and Bi (G) for Pt-Bi (Bi_2O_3)/GNs; The distribution of Pt and Bi (D) and Pt and Bi (H) atoms along the corresponding cross-sectional line shown in (A,E) respectively.

As indicated in the High-resolution transmission electron microscopy (HRTEM) images of Pt-Bi (Bi_2O_3)/GNs (PVP), Pt/GNs (PVP) and Pt-Bi (Bi_2O_3)/GNs (Figure 2C,F,I), lattice fringes with interplanar spacings of 0.227 nm corresponding to the (111) plane in the Pt fcc system were observed [35], which is in accordance with the XRD analysis. However, lattice fringes of Bi or Bi_2O_3 are not observed in Figure 2C,I, which may be because the Bi species in Pt-Bi (Bi_2O_3)/GNs (PVP) and Pt-Bi (Bi_2O_3)/GNs mainly exists in the form of Bi_2O_3 with poor crystallinity [25].

The HAADF-STEM of Pt-Bi (Bi_2O_3)/GNs (PVP) (Figure 3A) showed that the Pt-Bi nanoclusters were evenly distributed in the graphene layer and elemental mapping (Figure 3B–D) disclosed the homogeneous co-existence of Pt and Bi in the Pt-Bi nanoclusters. However, irregular Pt-Bi agglomerations were found in the HAADF-STEM of Pt-Bi (Bi_2O_3)/GNs (Figure 3E) and a similar co-existence of Pt and Bi was observed in elemental mappings (Figure 3F–H).

Figure 4 is a Raman spectrum of Pt-Bi (Bi_2O_3)/GNs (PVP), Pt/GNs (PVP) and Pt-Bi (Bi_2O_3)/GNs, which can be used to analyze the defects of the surface structure of the as-obtained GNs-based materials. As depicted in Figure 4, all samples exhibited two peaks at 1309 cm^{-1} and 1594 cm^{-1} , which were attributed to the D band and G band respectively. The intensity ratio of the D band and G band (I_D/I_G) is usually used to evaluate the extent of defects in carbonaceous materials. By calculation, the I_D/I_G ratios of Pt-Bi (Bi_2O_3)/GNs (PVP) (curve a), Pt/GNs (PVP) (curve b) and Pt-Bi (Bi_2O_3)/GNs (curve c) were 1.11, 1.11 and 1.18 respectively, which are similar to each other. This indicates that the introduction of different components (Pt, Bi or PVP) into graphene hardly changes the structural characteristics of graphene [33,36], which is helpful for graphene to retain its good electron transfer performance and to allow graphene-based materials to have better catalytic properties.

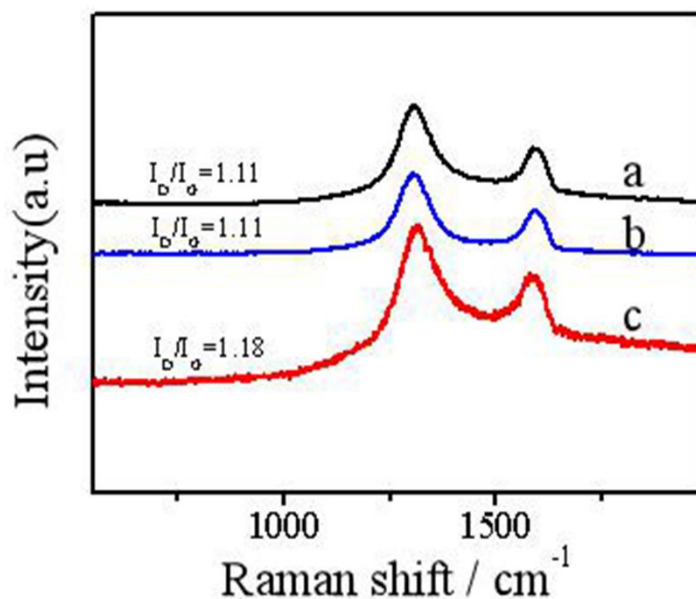


Figure 4. Raman spectra: Pt-Bi (Bi_2O_3)/GNs (PVP) (a), Pt/GNs (PVP) (b), Pt-Bi (Bi_2O_3)/GNs (c).

2.2. Electrocatalysis

Figure 5 shows the cyclic voltammetry curves of Pt-Bi (Bi_2O_3)/GNs (PVP) (curve a), 30% Johnson Matthey PtRu/C catalyst (30% PtRu/C-JM) (curve b), Pt/GNs (PVP) (curve c) and Pt-Bi (Bi_2O_3)/GNs (curve d) in a 1.0 M CH_3OH + 1.0 M NaOH solution. It can be clearly observed that the mass activities of Pt-Bi/GNs (PVP) ($1501.69 \text{ mA mg}^{-1}$) in the positive sweeps were 1.41 times, 2.88 times, and 11.01 times higher than those of commercial 30% PtRu/C-JM ($1068.74 \text{ mA mg}^{-1}$), Pt/GNs (PVP) ($521.58 \text{ mA mg}^{-1}$), and Pt-Bi (Bi_2O_3)/GNs ($136.39 \text{ mA mg}^{-1}$) respectively, demonstrating that Pt-Bi (Bi_2O_3)/GNs (PVP) had a significantly enhanced electrocatalytic activity for the MOR [33,37]. Furthermore, its mass activities were also higher than that of some reported Pt-based catalysts in an alkaline medium, such as spherical PtBi/glassy carbon electrode (GCE) catalyst (1400 mA mg^{-1}) [21], Pt/3D-GNs (PANI) catalyst (1172 mA mg^{-1}) [38] and Pt-Pd NPs/G catalyst (640 mA mg^{-1}) [39].

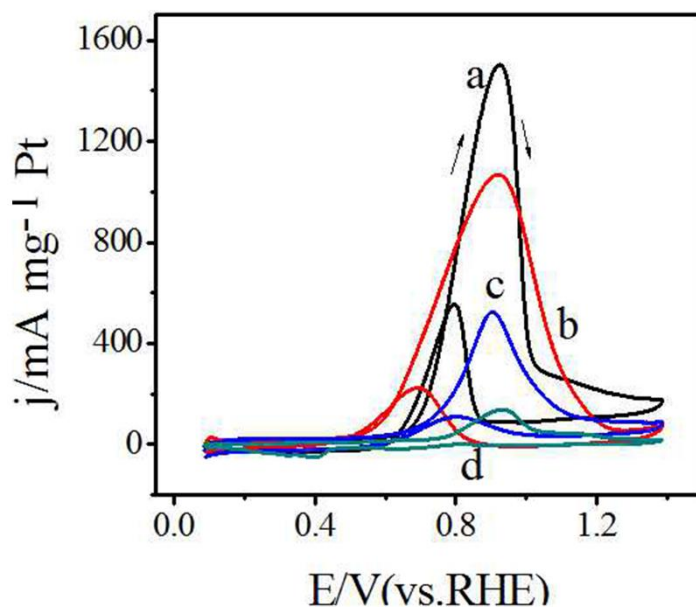


Figure 5. Cyclic voltammetry in 1.0 M CH_3OH + 1.0 M NaOH: Pt-Bi (Bi_2O_3)/GNs (PVP) (a), 30% PtRu/C-JM (b), Pt/GNs (PVP) (c) and Pt-Bi (Bi_2O_3)/GNs (d), at 10 mV s^{-1} .

The chronoamperometry curve carried out at 0.7 V for 2000 s was used to further explore the catalytic stability of the as-tested catalysts. It can be seen from Figure 6 that the Pt-Bi (Bi₂O₃)/GNs (PVP) had a relatively higher initial current density, a slower decrease and a higher steady-state current density, indicating better catalytic stability of Pt-Bi (Bi₂O₃)/GNs (PVP) for catalyzing methanol oxidation. In particular, the decay of the current density for Pt-Bi (Bi₂O₃)/GNs (PVP) was slightly slower than that of 30% PtRu/C-JM. The better catalytic performance of Pt-Bi (Bi₂O₃)/GNs (PVP) towards the MOR may be attributed to the following bifunctional mechanism: Firstly, the introduction of PVP can promote the uniform distribution of Pt and Bi particles on a graphene surface, as shown in Figure 2, which effectively improves its catalytic activity. Secondly, due to surface oxidation caused by oxophilic Bi, a large amount of OH_{ads} formed on the catalyst surface. OH_{ads} can react with intensively adsorbed species such as low potential CO, to release dissociative Pt active sites for further oxidizing methanol molecules. As for Pt-Bi (Bi₂O₃)/GNs, the poor dispersion of the Pt-Bi nanoparticles was responsible for its inferior performance.

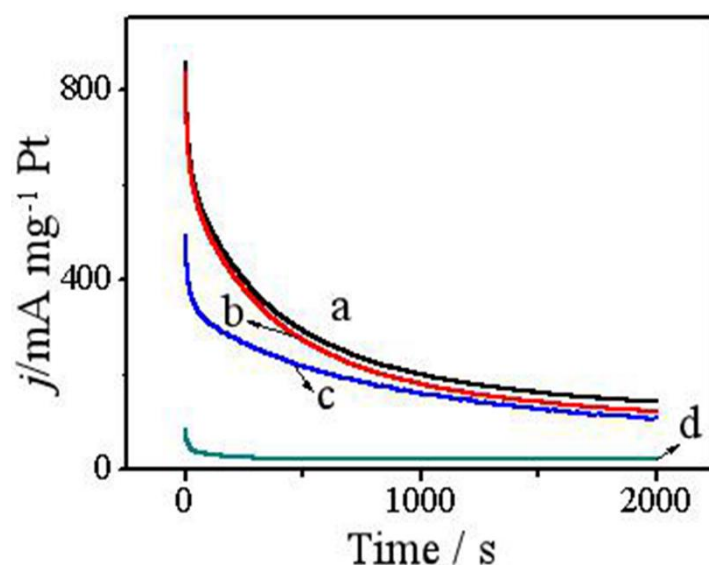


Figure 6. Chronoamperometric curves in 1.0 M CH₃OH + 1.0 M NaOH: Pt-Bi (Bi₂O₃)/GNs (PVP) (a), 30% PtRu/C-JM (b), Pt/GNs (PVP) (c), and Pt-Bi (Bi₂O₃)/GNs (d), at 100 mV s⁻¹.

Pt-Bi (Bi₂O₃)/GNs (PVP) and Pt-Bi (Bi₂O₃)/GNs were also investigated as potential electrocatalysts towards the oxygen reduction reaction (ORR). As for the ORR, cyclic voltammetry was firstly performed in a 1.0 M NaOH solution saturated with N₂. It was obvious that there was a peak around 0.40 V versus the reversible hydrogen electrode (RHE) (in Figure 7A,D) in the backward scanning curves, which was associated with the presence of Bi [40]. After that, cyclic voltammetry was carried out in a 1.0 M NaOH solution saturated with O₂. Among all of the tested catalysts, Pt-Bi (Bi₂O₃)/GNs (PVP) had a significant oxygen reduction peak current density with the value of -7.85 mA mg⁻¹ in an oxygen saturated 1.0 M NaOH solution (curve a in Figure 7A), which was 1.03 times, 1.67 times, 1.30 times higher than that of 30% PtRu/C-JM (-7.63 mA mg⁻¹), Pt/GNs (PVP) (-4.70 mA mg⁻¹) and Pt-Bi (Bi₂O₃)/GNs (-6.02 mA mg⁻¹) respectively. Furthermore, the reduction peak potential of Pt-Bi (Bi₂O₃)/GNs (PVP) was at 0.82 V versus RHE, which was more positive than that of commercial 30% PtRu/C-JM (0.78 V), Pt/GNs (PVP) (0.79 V) and Pt-Bi (Bi₂O₃)/GNs (0.71 V). Obviously, Pt-Bi (Bi₂O₃)/GNs (PVP) exhibited superior catalytic activities for the ORR, confirming that the introduction of Bi can improve the catalytic activity of oxygen reduction.

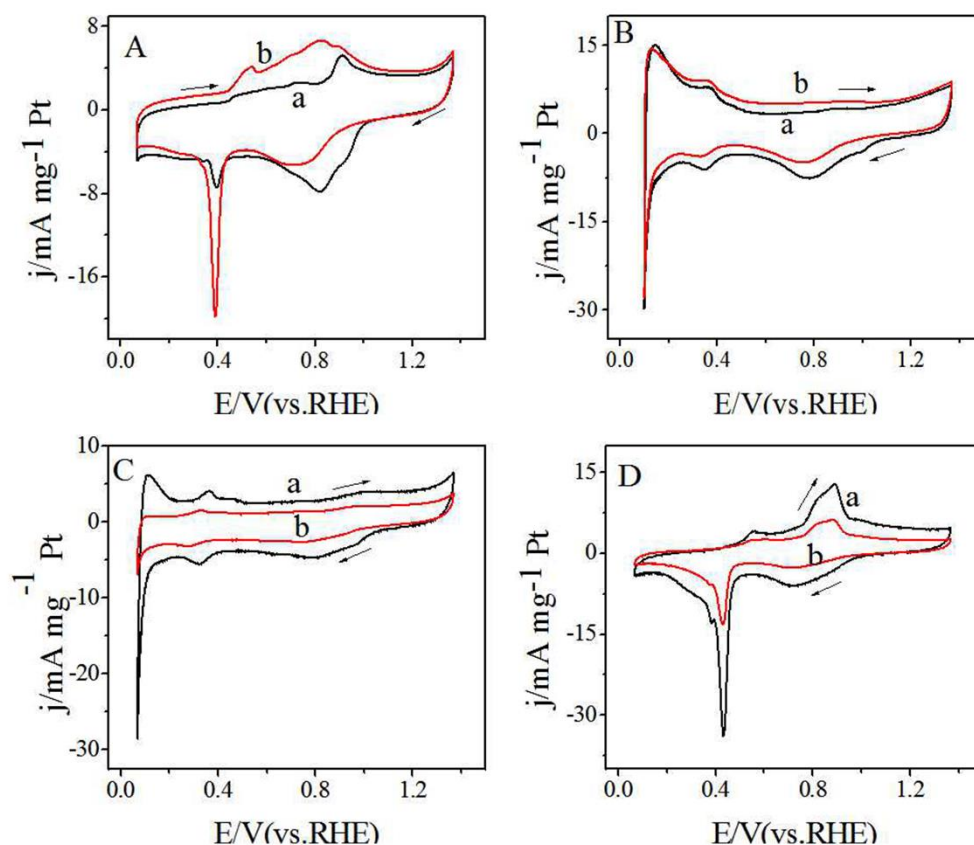


Figure 7. Cyclic voltammetry in 1.0 M NaOH: Pt-Bi (Bi_2O_3)/GNs (PVP) (A), 30% PtRu/C-JM (B), Pt/GNs (PVP) (C) and Pt-Bi (Bi_2O_3)/GNs (D), at 10 mV s^{-1} , curve a: saturated with oxygen, curve b: saturated with nitrogen.

To further evaluate their catalytic properties towards the ORR, a linear sweep voltammetry test was conducted using a rotating disk electrode, which is shown in Figure 8. It was found that with an increase in the electrode rotational speed, the limited current density of the oxygen reduction reaction was augmented linearly. The corresponding slopes of the Koutecky-Levich plots obtained from the inverse current density (j^{-1}) as a function of the inverse of the square root of the rotation rate ($\omega^{-1/2}$) at diverse potentials were used to calculate their electron transfer number on the basis of the following Koutecky-Levich equation [41].

$$1/j = 1/j_L + 1/j_K = 1/(B\omega^{1/2}) + 1/j_K, \quad (1)$$

$$B = 0.62 nFC_0(D_0)^{2/3}v^{-1/6}. \quad (2)$$

It was calculated that the average electron transfer number during the catalysis of the ORR for the Pt-Bi (Bi_2O_3)/GNs (PVP) was 3.56, indicating that O_2 on the surface of Pt-Bi (Bi_2O_3)/GNs (PVP) was substantially reduced by the four-electron-transfer pathway, which was close to that of 30% PtRu/C-JM. In contrast, the average electron transfer number of Pt/GNs (PVP) and Pt-Bi (Bi_2O_3)/GNs was 1.83 and 2.65, respectively, further confirming that Pt-Bi (Bi_2O_3)/GNs (PVP) was more selective for catalyzing the oxygen reduction reaction.

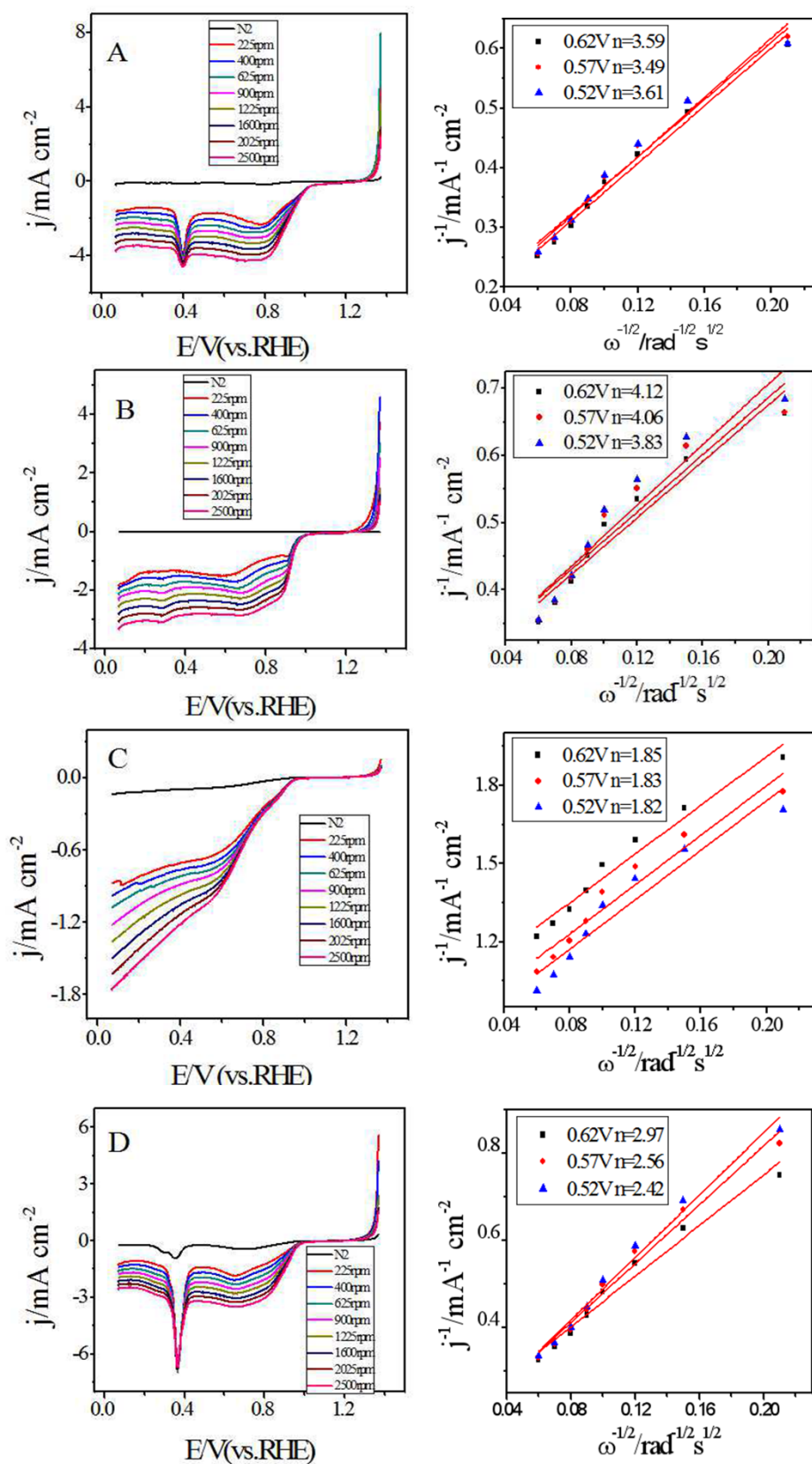


Figure 8. Linear scanning voltammetry (LSV) curves for the Pt-Bi (Bi_2O_3)/GNs (PVP) (A), 30% PtRu/C-JM (B), Pt/GNs (PVP) (C), Pt-Bi (Bi_2O_3)/GNs (D) in an O_2 saturated 1.0 M NaOH solution at different rotation rates.

In view of the photo-responsive properties of Bi_2O_3 , the electro-photo catalysis of the as-synthesized composites for the MOR and the ORR under simulated sunlight was investigated. As for the MOR, cyclic voltammetry measurements of different modified electrodes were carried out under simulated sunlight irradiation in a 1.0 M CH_3OH + 1.0 M NaOH solution. The results in Figure 9 revealed that the Pt-Bi (Bi_2O_3)/GNs (PVP) composite exhibited a distinctly increasing mass activity with the value of $2129.18 \text{ mA mg}^{-1}$ under the simulated sunlight irradiation, which was 1.42 times higher than that without irradiation. In contrast, Pt/GNs (PVP) and 30% PtRu/C-JM exhibited weak electro-photo catalytic activity. Hence, it is reasonable to conclude that the photosensitivity of the Bi species (especially Bi_2O_3) in Pt-Bi (Bi_2O_3)/GNs (PVP) resulted in a significant increase in activity for catalyzing the MOR. As for Pt-Bi (Bi_2O_3)/GNs, the poor distribution of the Pt-Bi agglomerations also resulted in an inferior electro-photo catalytic activity for the MOR.

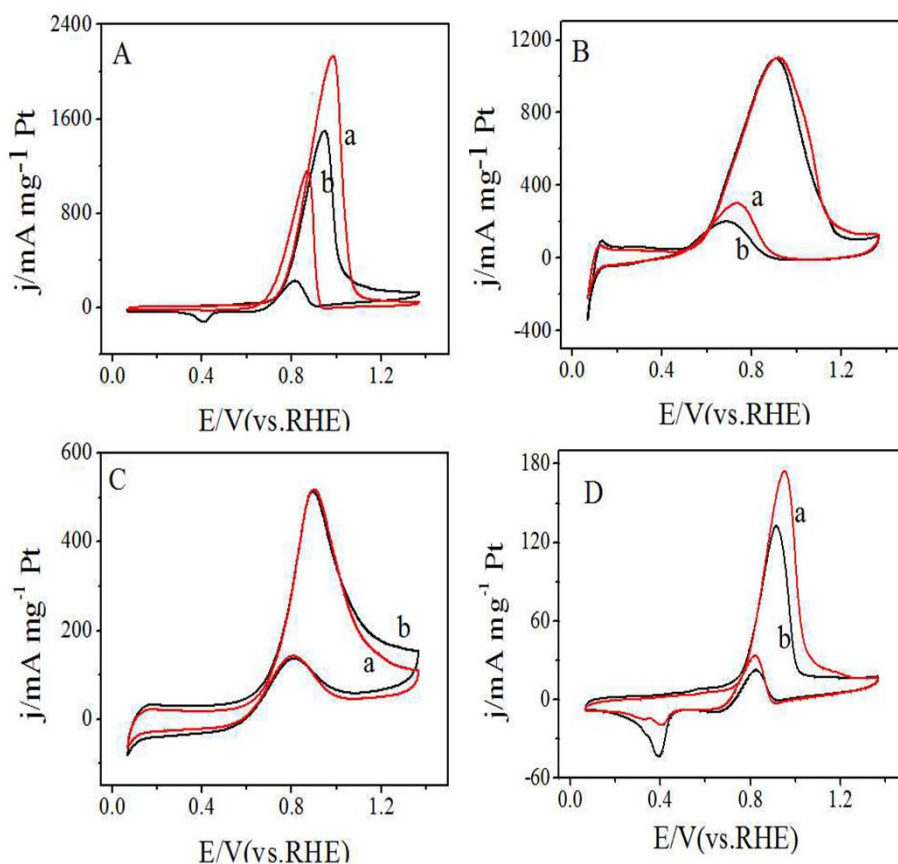


Figure 9. Cyclic voltammetry in 1.0 M CH_3OH + 1.0 M NaOH : Pt-Bi (Bi_2O_3)/GNs (PVP) (A), 30% PtRu/C-JM (B), Pt/GNs (PVP) (C), Pt-Bi (Bi_2O_3)/GNs (D); curve a: with simulator sunlight irradiation, curve b: without irradiation.

Similarly, the effect of simulated sunlight irradiation on the ORR was examined. Figure 10A shows that Pt-Bi (Bi_2O_3)/GNs (PVP) exhibited a prominently increasing mass activity with the value of $-13.08 \text{ mA mg}^{-1}$ under simulated sunlight irradiation, which was 1.67 times higher than that without irradiation. Furthermore, its potential reduction peak positively shifted under light irradiation, changing from 0.82 V (without irradiation) to 0.83 V (under light irradiation). Nevertheless, only a slight increase in the mass activity occurred for the other samples.

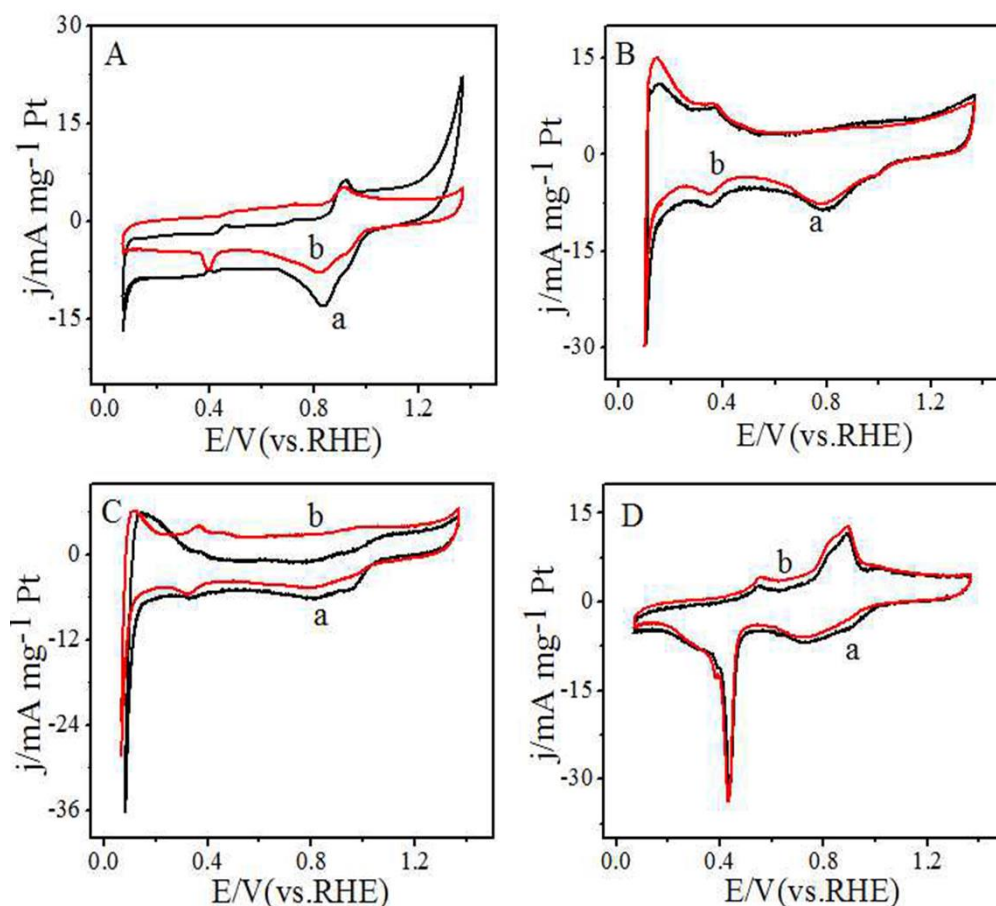


Figure 10. Cyclic voltammetry in 1.0 M NaOH saturated with oxygen: Pt-Bi (Bi_2O_3)/GNs (PVP) (A), 30% PtRu/C-JM (B), Pt/GNs (PVP) (C) and Pt-Bi (Bi_2O_3)/GNs (D), curve a: under simulated sunlight irradiation, curve b: without irradiation.

Obviously, the electro-photo catalysis of Pt-Bi (Bi_2O_3)/GNs (PVP) for the MOR and the ORR was due to the existence of the photo-responsive Bi species (mainly Bi_2O_3) and a better dispersion of Pt-Bi (Bi_2O_3)/GNs (PVP) in response to the tuning role of PVP. As shown in Figure 11, when the external light irradiated onto the surface of Pt-Bi (Bi_2O_3)/GNs (PVP), electron-hole pairs were generated by the photo-excited Bi_2O_3 and the photo-generated electron transferred to the surface of Pt via the well-dispersed structure of graphene to refresh the Pt active sites ($\text{PtO}_x + \text{photo-generated } e^- \rightarrow \text{Pt}$ during the MOR) or to participate in catalyzing the reaction ($\text{O}_2 + \text{photo-generated } e^- \rightarrow 2\text{O}^{2-}$ during the ORR) [42], so that the synergistic interaction between the electrocatalytic properties and the photocatalytic properties of Pt-Bi (Bi_2O_3)/GNs (PVP) for the MOR and the ORR can be achieved.

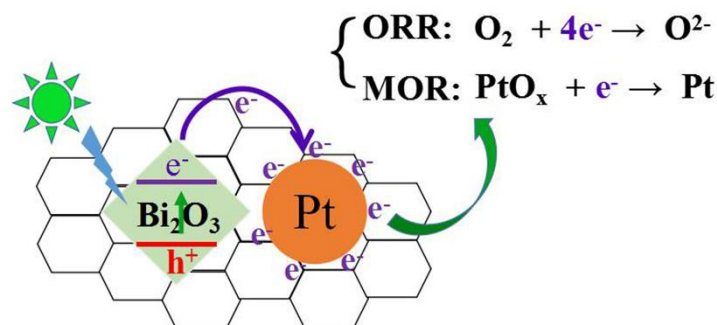


Figure 11. The electro-photo catalytic mechanism for the methanol oxidation reaction (MOR) and the oxygen reduction reaction (ORR).

3. Experimental

3.1. Materials

Graphite powder (−325 mesh, 99.9995%) was purchased from the Alfa Aesar Company (Ward Hill, MA, USA); 5% Nafion 117 solution and 30% PtRu/C-JM catalyst were obtained from Johnson-Matthey (London, UK); Bi(NO₃)₃, NaBH₄, Pt(NO₃)₂, PVP, methanol, ethanol, KMnO₄, H₂SO₄, H₂O₂ (30%), P₂O₅, K₂S₂O₈, acetone were all purchased from Sinopharm Chemical Reagent Co, Ltd. (Shanghai, China) and used without further purification. Ultrapure water for the laboratory was 18.25 MΩ cm deionized water, deoxygenated with nitrogen before use.

3.2. Synthesis of Pt-Bi (Bi₂O₃)/GNs (PVP)

Graphite oxide (GO) was synthesized from natural graphite powder using the modified Hummers' method [43,44]. In general, graphite was oxidized with concentrated H₂SO₄ (98%), K₂S₂O₄, P₂O₅, and KMnO₄. After oxidation, H₂O₂ (30%) was added. The product was centrifuged and washed with 5% dilute HCl solution and deionized water several times. Then the GO suspension was dialyzed for one week with a BIOSHARP membrane (MW: 8000–1400) [42]. After centrifugation, the brown precipitate (GO) was lyophilized for the following utilization. The overall synthetic route of Pt-Bi (Bi₂O₃)/GNs (PVP) was as follows: 58.2 mg of Bi(NO₃)₃·5H₂O was dissolved in 50 mL of water, then 40 mg of PVP powder was added to the mixture and stirred for 30 min. Meanwhile, 60 mg of GO was dispersed in 30 mL of distilled water by sonication for 30 min. Afterwards, the GO suspension was added to the above mixture and stirred for 15 min. After that, 5 mL NaBH₄ (24 mM) was added to the solution via a deposition reaction for 1 h. The mixture was placed in an oil bath and heated to 80 °C to decompose the remaining NaBH₄. Next, 2 mL of Pt(NO₃)₂ (10 mL/100 mL) was added into the solution above and stirred for another 30 min. Then, 2 mL HCOOH was put in and reacted at room temperature for 48 h to finally obtain a black precipitate. Subsequently, the black product was isolated using a high-speed centrifuge (12,000 rpm, 10 min) and deionized water washing cycles (five cycles). Ultimately, the purified precipitate was dried in a vacuum freeze dryer for 48 h. The counterparts Pt/GNs (PVP) and Pt-Bi (Bi₂O₃)/GNs were synthesized using a similar procedure. The contents of Pt and Bi in the Pt-Bi (Bi₂O₃)/GNs (PVP) and Pt-Bi (Bi₂O₃)/GNs composites were determined by ICP-AES. The actual contents of Pt and Bi were 20.67% and 23.07% and 19.75% and 28.41%, respectively. The Pt content of Pt/GNs (PVP) composite was 21.58%.

3.3. Characterization

High-resolution transmission electron microscopy (HRTEM, TECNAI G2, FEI Company, Hillsboro, OR, USA), was used to observe the morphology of composites; X-ray photoelectron spectroscopy (XPS, VG ESCALAB 250, Thermo Scientific, Pleasanton, CA, USA, Al-Kα radiation (1486.6 eV)) was used to analyze the surface components of the catalysts; the XRD patterns were carried out using X-ray diffraction (XRD, X'pert Pro, PANalytical B.V., Holland, The Netherlands, Cu-Kα radiation); the metal content in the composite was determined using an Inductively Coupled Plasma Atomic Emission Spectrometer (ICP-AES, ICAP6300, Thermo Scientific, Pleasanton, CA, USA); the structure of graphene in the composite was analyzed by Raman spectroscopy (Via-Reflex, Renishaw, London, UK).

3.4. Electrochemical Measurements

All electrochemical experiments were performed at room temperature using a standard three-electrode electrochemical workstation. Electrochemical tests were performed on electrochemical workstations (CH Instruments, Shanghai, China). A Calomel electrode (SCE, saturated KCl) and a platinum column were the reference electrode and the counter electrode respectively. The glassy carbon electrode was the working electrode, which was firstly hand-polished with 0.05 μm α-Al₂O₃ polishing powder and rinsed with deionized water, followed by sonication in ethanol and deionized water.

After pre-treatment, the working electrode was modified according to the following steps: 5 mg of the composite material was ultrasonically dispersed into 1 mL C₂H₅OH, next 5 µL of the composite solution was dropped onto the glassy carbon electrode and dried in air. Then, 7.5 µL of a Nafion (0.5%) solution was added. Cyclic voltammetry (CV) for the methanol oxidation reaction (MOR) was performed in a 1.0 M NaOH or 1.0 M NaOH + 1.0 M CH₃OH solution at a scanning rate of 100 mV·s⁻¹ at room temperature. Linear sweep cyclic voltammetry (LSV) for the oxygen oxidation reaction (ORR) was tested in a 1.0 M NaOH solution at a scanning rate of 5 mV·s⁻¹ at room temperature.

For the electro-photo catalysis tests: A quartz window was introduced at the bottom of the electrochemical cell, facing towards the working electrode. A 15 W Xenon lamp (ZW3D15WZ105, Cnlight, Foshan, China) was used to provide UV light or visible light by changing the different optical filters. The irradiation light could penetrate through the quartz window and illuminate the surface of GCE. The lamp emitted simulated solar light of wavelengths ranging from 200 to 800 nm. The distance between the GCE and the lamp was 15 cm and the irradiation intensity was 0.3 mW cm².

4. Conclusions

In summary, the Pt-Bi (Bi₂O₃)/GNs (PVP) composite was obtained by aqueous solution synthesis with the aid of the morphology tuning PVP. It was tested as a superior bifunctional electrocatalyst towards the MOR and the ORR. While catalyzing the MOR, the introduction of oxophilic Bi resulted in an increasing OH_{ads} species on the Pt surface, which was in favor for the further oxidation of CO_{ads}. On the other hand, Pt-Bi (Bi₂O₃)/GNs (PVP) exhibited a more selective and effective catalytic activity for the oxygen reduction reaction using an approximately four-electron-transfer pathway. In particular, under simulated light irradiation, the photo-sensitivity of Bi₂O₃ led to a significant increase in the activity of Pt-Bi (Bi₂O₃)/GNs (PVP) for catalyzing both the MOR and the ORR. This study is beneficial to exploiting novel bifunctional catalysts with an excellent electro-photo catalytic activity for DMFCs application.

Author Contributions: Z.L. planned and designed the experiments; Y.W., X.D. and Y.L. performed the experimental work; Z.L., S.X. and Y.X. contributed to the data analysis; Y.W. and X.D. wrote the manuscript; Z.L. revised the manuscript; S.L. supervised the project and revised the manuscript; all authors discussed the results and approved of the final version of the manuscript.

Funding: This work was financially supported by the National Natural Science Foundation of China (Nos. 21171037 & 21571034) and the Research Foundation from Quangang Petrochemical Research Institute of Fujian Normal University (No. 2016YJY05).

Conflicts of Interest: The authors declare no conflict of interest.

References

1. Zhong, C.J.; Luo, J.; Fang, B.; Wanjala, B.N.; Njoki, P.N.; Loukrakpam, R.; Yin, J. Nanostructured catalysts in fuel cells. *Nanotechnology* **2010**, *21*, 062001. [[CrossRef](#)] [[PubMed](#)]
2. Xiao, L.; Zhuang, L.; Liu, Y.; Lu, J.; Abruña, H.D. Activating Pd by morphology tailoring for oxygen reduction. *J. Am. Chem. Soc.* **2009**, *131*, 602–608. [[CrossRef](#)] [[PubMed](#)]
3. Guo, S.; Wang, E. Noble metal nanomaterials: Controllable synthesis and application in fuel cells and analytical sensors. *Nano Today* **2011**, *6*, 240–264. [[CrossRef](#)]
4. He, L.L.; Zheng, J.N.; Pei, S.; Zhong, S.X.; Wang, A.J.; Chen, Z.; Feng, J.J. Facile synthesis of platinum–gold alloyed string-bead nanochain networks with the assistance of allantoin and their enhanced electrocatalytic performance for oxygen reduction and methanol oxidation reactions. *J. Power Sources* **2015**, *276*, 357–364. [[CrossRef](#)]
5. Freitas, R.G.; Pereira, E.C. Giant multilayer electrocatalytic effect investigation on Pt/Bi/Pt nanostructured electrodes towards CO and methanol electrooxidation. *Electrochim. Acta* **2010**, *55*, 7622–7627. [[CrossRef](#)]
6. Bahrami, K.; Kamrani, S.N. Synthesis, characterization and application of graphene palladium porphyrin as a nanocatalyst for the coupling reactions such as: Suzuki-miyaura and Mizoroki-Heck: Synthesis, characterization and application of graphene palladium. *Appl. Organomet. Chem.* **2018**, *32*, e4102. [[CrossRef](#)]

7. Xiao, Z.; Zhu, J.; Cai, W.; Xiao, M.; Liang, L.; Liu, C.; Wei, X. Pt–Pb hollow sphere networks: Self-sacrifice-templating method and enhanced activity for formic acid electrooxidation. *Rsc Adv.* **2013**, *3*, 1763–1767.
8. Min, Y.; Huang, Y.; Lv, Q.; Liang, L.; Liao, J.; Liu, C.; Wei, X. Improved direct electrooxidation of formic acid by increasing au fraction on the surface of ptau alloy catalyst with heat treatment. *Electrochim. Acta* **2011**, *58*, 6–11.
9. Chen, T.; Ge, C.; Zhang, Y.; Zhao, Q.; Hao, F.; Bao, N. Bimetallic platinum–bismuth nanoparticles prepared with silsesquioxane for enhanced electrooxidation of formic acid. *Int. J. Hydrog. Energy* **2015**, *40*, 4548–4557. [[CrossRef](#)]
10. Cao, J.; Du, Y.; Dong, M.; Chen, Z.; Xu, J. Template-free synthesis of chain-like ptcu nanowires and their superior performance for oxygen reduction and methanol oxidation reaction. *J. Alloy. Compd.* **2018**, *747*, 124–130. [[CrossRef](#)]
11. Liu, S.H.; Zheng, F.S.; Wu, J.R. Preparation of ordered mesoporous carbons containing well-dispersed and highly alloying pt-co bimetallic nanoparticles toward methanol-resistant oxygen reduction reaction. *Appl. Catal. B Environ.* **2011**, *108*, 81–89. [[CrossRef](#)]
12. Chen, W.; Kim, J.; Sun, S.; Chen, S. Electro-oxidation of formic acid catalyzed by fept nanoparticles. *Phys. Chem. Chem. Phys.* **2006**, *8*, 2779–2786. [[CrossRef](#)] [[PubMed](#)]
13. Habibi, B.; Delnavaz, N. Carbon–ceramic supported bimetallic Pt–Ni nanoparticles as an electrocatalyst for oxidation of formic acid. *Int. J. Hydrog. Energy* **2011**, *36*, 9581–9590. [[CrossRef](#)]
14. Xu, C.; Hou, J.; Pang, X.; Li, X.; Zhu, M.; Tang, B. Nanoporous ptco and ptni alloy ribbons for methanol electrooxidation. *Int. J. Hydrog. Energy* **2012**, *37*, 10489–10498. [[CrossRef](#)]
15. Roychowdhury, C.; Matsumoto, F.; Mutolo, P.F.; Abruna, H.D.; Disalvo, F.J. Synthesis, characterization, and electrocatalytic activity of PtBi nanoparticles prepared by the polyol process. *Chem. Mater.* **2005**, *23*, 5871–5876. [[CrossRef](#)]
16. Ding, L.X.; Li, G.R.; Wang, Z.L.; Liu, Z.Q.; Liu, H.; Tong, Y.X. Porous Ni@Pt core-shell nanotube array electrocatalyst with high activity and stability for methanol oxidation. *Chem. A Eur. J.* **2012**, *18*, 8386–8391. [[CrossRef](#)] [[PubMed](#)]
17. Peng, X.; Zhao, Y.; Chen, D.; Fan, Y.; Wang, X.; Wang, W.; Tian, J. One-pot synthesis of reduced graphene oxide supported ptcu y catalysts with enhanced electro-catalytic activity for the methanol oxidation reaction. *Electrochim. Acta* **2014**, *136*, 292–300. [[CrossRef](#)]
18. Kannan, R.; Silva, A.A.; Cardoso, F.M.; Gupta, G.; Aslam, Z.; Sharma, S.; Steinbergerwilckens, R. Study of fept deposited reduced graphene oxide’s utility as a catalyst towards oxygen reduction and methanol oxidation reactions. *Rsc Adv.* **2015**, *5*, 36993–36998. [[CrossRef](#)]
19. Qin, Y.; Zhang, X.; Dai, X.; Sun, H.; Yang, Y.; Li, X.; Shi, Q.; Gao, D.; Wang, H.; Yu, N.F. Graphene oxide-assisted synthesis of Pt-Co alloy nanocrystals with high-index facets and enhanced electrocatalytic properties. *Angew. Chem. Int. Ed.* **2015**, *53*, 12522–12527. [[CrossRef](#)] [[PubMed](#)]
20. Huang, Y.; Cai, J.; Guo, Y. Facile synthesis of a Bi-modified PtRu catalyst for methanol and ethanol electro-oxidation in alkaline medium. *Int. J. Hydrog. Energy* **2013**, *38*, 3250–3256. [[CrossRef](#)]
21. Yang, M. Catalytic activities of ptbi nanoparticles toward methanol electrooxidation in acid and alkaline media. *J. Power Sources* **2013**, *229*, 42–47. [[CrossRef](#)]
22. Nuñez-Briones, A.G.; García-Cerda, L.A.; Aguilar-González, M.A.; Puente-Urbina, B.A.; Mendoza-Mendoza, E. Synthesis, structural characterization and photocatalytic activity of Bi-based nanoparticles. *Int. J. Appl. Ceram. Technol.* **2017**, *15*, 101–110. [[CrossRef](#)]
23. Li, Z.; Ye, L.; Wang, Y.; Xu, S.; Lei, F.; Lin, S. Visible light assisted electro-photo synergistic catalysis of heterostructured Pd-Ag nps/graphene for methanol oxidation. *Rsc Adv.* **2016**, *6*, 79533–79541. [[CrossRef](#)]
24. Li, Z.; Zhang, L.; Huang, X.; Ye, L.; Lin, S. Shape-controlled synthesis of Pt nanoparticles via integration of graphene and β -cyclodextrin and using as a noval electrocatalyst for methanol oxidation. *Electrochim. Acta* **2014**, *121*, 215–222. [[CrossRef](#)]
25. Li, Z.; Xu, S.; Xie, Y.; Wang, Y.; Lin, S. Promotional effects of trace Bi on its highly catalytic activity for methanol oxidation of hollow pt/graphene catalyst. *Electrochim. Acta* **2018**, *264*, 53–60. [[CrossRef](#)]
26. Li, S.S.; Lv, J.J.; Teng, L.N.; Wang, A.J.; Chen, J.R.; Feng, J.J. Facile synthesis of PdPt@Pt nanorings supported on reduced graphene oxide with enhanced electrocatalytic properties. *Acs Appl. Mater. Interfaces* **2014**, *6*, 10549–10555. [[CrossRef](#)] [[PubMed](#)]

27. Cai, J.; Huang, Y.; Guo, Y. Bi-modified Pd/C catalyst via irreversible adsorption and its catalytic activity for ethanol oxidation in alkaline medium. *Electrochim. Acta* **2013**, *99*, 22–29. [[CrossRef](#)]
28. Xie, Y.; Li, Z.; Wang, Y.; Xu, S.; Lin, S. Freezing synthesis of Pt/3D GNs (C) composites as efficient electrocatalysts for methanol oxidation. *J. Appl. Electrochem.* **2018**, *48*, 1–10. [[CrossRef](#)]
29. You, H.; Zhang, F.; Liu, Z.; Fang, J. Free-standing Pt–Au hollow nanourchins with enhanced activity and stability for catalytic methanol oxidation. *ACS Catal.* **2014**, *4*, 2829–2835. [[CrossRef](#)]
30. Lei, F.; Li, Z.; Zhang, L.; Wang, Y.; Xu, S.; Lin, S. Facile synthesis of Pt–Cu (Ni, Co)/GNs–CD and their enhanced electro-catalytic activity for methanol oxidation. *J. Electrochem. Soc.* **2016**, *163*, F913–F918. [[CrossRef](#)]
31. Naterer, G.F.; Suppiah, S.; Stolberg, L.; Lewis, M.; Ferrandon, M.; Wang, Z.; Dincer, I.; Gabriel, K.; Rosen, M.A.; Secnik, E. Clean hydrogen production with the Cu–Cl cycle—progress of international consortium, i: Experimental unit operations. *Int. J. Hydrog. Energy* **2011**, *36*, 15472–15485. [[CrossRef](#)]
32. Huang, Y.; Cai, J.; Liu, M.; Guo, Y. Fabrication of a novel PtPbBi/C catalyst for ethanol electro-oxidation in alkaline medium. *Electrochim. Acta* **2012**, *83*, 1–6. [[CrossRef](#)]
33. Yu, X.; Pickup, P.G. Carbon supported PtBi catalysts for direct formic acid fuel cells. *Electrochim. Acta* **2011**, *56*, 4037–4043. [[CrossRef](#)]
34. Neto, A.O.; Tusi, M.M.; Polanco, N.S.D.O.; Silva, S.G.D.; Santos, M.C.D.; Spinacé, E.V. PdBi/C electrocatalysts for ethanol electro-oxidation in alkaline medium. *Int. J. Hydrog. Energy* **2011**, *36*, 10522–10526. [[CrossRef](#)]
35. Park, J.Y.; Kim, S. Preparation and electroactivity of polymer-functionalized graphene oxide-supported platinum nanoparticles catalysts. *Int. J. Hydrog. Energy* **2013**, *38*, 6275–6282. [[CrossRef](#)]
36. Yang, J.; Ying, X.; Wang, R.; Jiang, B.; Tian, C.; Mu, G.; Jie, Y.; Bo, W.; Fu, H. Synergistic effect of tungsten carbide and palladium on graphene for promoted ethanol electrooxidation. *Appl. Mater. Interfaces* **2013**, *5*, 6571–6579. [[CrossRef](#)] [[PubMed](#)]
37. Huang, Y.; Cai, J.; Guo, Y. A high-efficiency microwave approach to synthesis of Bi-modified Pt nanoparticle catalysts for ethanol electro-oxidation in alkaline medium. *Appl. Catal. B Environ.* **2013**, *129*, 549–555. [[CrossRef](#)]
38. Wang, Y.; Li, Z.; Xu, S.; Xie, Y.; Lin, S. Highly dispersive platinum nanoparticles supporting on polyaniline modified three dimensional graphene and catalyzing methanol oxidation. *Mater. Res. Bull.* **2018**, *102*, 172–179. [[CrossRef](#)]
39. Zhang, Y.; Chang, G.; Shu, H.; Oyama, M.; Liu, X.; He, Y. Synthesis of Pt–Pd bimetallic nanoparticles anchored on graphene for highly active methanol electro-oxidation. *J. Power Sources* **2014**, *262*, 279–285. [[CrossRef](#)]
40. Yovanovich, M.; Piasentin, R.M.; Ayoub, J.M.S.; Nandenha, J.; Fontes, E.H.; Souza, R.F.B.D.; Buzzo, G.S.; Silva, J.C.M.; Spinacé, E.V.; Assumpção, M.H.M.T. PtBi/C electrocatalysts for formic acid electro-oxidation in acid and alkaline electrolyte. *Int. J. Electrochem. Sci.* **2015**, *10*, 4801–4811.
41. Yang, Z.; Zhou, X.; Nie, H.; Yao, Z.; Huang, S. Facile construction of manganese oxide doped carbon nanotube catalysts with high activity for oxygen reduction reaction and investigations into the origin of their activity enhancement. *ACS Appl. Mater. Interfaces* **2011**, *3*, 2601–2606. [[CrossRef](#)] [[PubMed](#)]
42. Li, Z.; Ye, L.; Lei, F.; Wang, Y.; Xu, S.; Lin, S. Enhanced electro-photo synergistic catalysis of Pt (Pd)/ZnO/graphene composite for methanol oxidation under visible light irradiation. *Electrochim. Acta* **2016**, *188*, 450–460. [[CrossRef](#)]
43. Zeng, Q.; Cheng, J.; Tang, L.; Liu, X.; Liu, Y.; Li, J.; Jiang, J. Self-assembled graphene–enzyme hierarchical nanostructures for electrochemical biosensing. *Adv. Funct. Mater.* **2010**, *20*, 3366–3372. [[CrossRef](#)]
44. Hummers, W.S., Jr.; Offeman, R.E. Preparation of graphitic oxide. *J. Am. Chem. Soc.* **1958**, *80*, 1339. [[CrossRef](#)]

